ACS APPLIED MATERIALS & INTERFACES

Research Article

www.acsami.org

Realization of Both High-Performance and Enhanced Durability of Fuel Cells: Pt-Exoskeleton Structure Electrocatalysts

Ok-Hee Kim,[†] Yoon-Hwan Cho,[‡,§] Tae-Yeol Jeon,[∥] Jung Won Kim,[⊥] Yong-Hun Cho,*[,⊥] and Yung-Eun Sung*[,‡,§]

[†]Department of Science, Republic of Korea Naval Academy, Jinhae-gu, Changwon 645-797, South Korea

[‡]Center for Nanoparticle Research, Institute for Basic Science (IBS), Seoul 151-747, South Korea

[§]School of Chemical and Biological Engineering, Seoul National University, Seoul 151-747, South Korea

[∥]Pohang Accelerator Laboratory, Pohang University of Science and Technology, Pohang 790-784, South Korea

[⊥]Department of Chemical Engineering, Kangwon National University, Samcheok 245-711, South Korea

Supporting Information

ABSTRACT: Core−shell structure nanoparticles have been the subject of many studies over the past few years and continue to be studied as electrocatalysts for fuel cells. Therefore, many excellent core−shell catalysts have been fabricated, but few studies have reported the real application of these catalysts in a practical device actual application. In this paper, we demonstrate the use of platinum (Pt)-exoskeleton structure nanoparticles as cathode catalysts with high stability and remarkable Pt mass activity and report the outstanding performance of these materials when used in membrane-electrode assemblies (MEAs) within a polymer electrolyte membrane fuel cell. The stability and degradation characteristics of these materials were also investigated in single cells in an accelerated degradation test using load cycling, which is similar to the drive cycle of a polymer electrolyte membrane fuel cell used in vehicles. The MEAs with Pt-exoskeleton structure catalysts showed enhanced performance throughout the single cell test and exhibited improved degradation ability that differed from that of a commercial Pt/C catalyst.

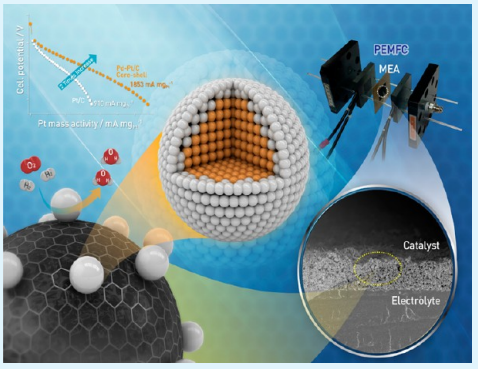

KEYWORDS: *fuel cells, core/shell nanoparticles, electrocatalysts, membrane electrode assemblies, degradation*

1. INTRODUCTION

The cost and scarcity of novel metals, especially platinum (Pt), is one of the most significant barriers to the commercialization of polymer electrolyte membrane fuel cells (PEMFCs).[1] Several methods have been studied for replacing expensive Pt-based catalysts, to reduce the cost of electrode materials, increase Pt usage efficiency through alloying, construct core−shell structures with cheaper metals, or facet the active Pt surfaces. Many reports have been published on nonprecious metal catalysts, but only a few papers have realistically demonstrated the use of these materials in practical fuel cells.[2,3] Studies of core−shell structure catalysts have typically received considerable attention for fuel cell applications because of the numerous advantages associated with these materials, such as their outstanding activity and stability.[4,5] In addition, the core−shell structure can reduce the cost of the catalyst because a low-cost metal is used for the core, and a rare metal is used for the shell. Also, the structure affects the catalytic activity and the dispersion of the core−shell particles. Palladium (Pd)-based bimetallic catalysts have received particular attention because Pd and Pt belong to the same group within the periodic table and therefore have similar properties. These elements have the same face-centered cubic (fcc) crystal structure and similar atomic sizes. However, Pd is cheaper than Pt and more abundant in the earth's crust. Furthermore, significant electrocatalytic activity has been reported for Pd-based core−shell catalysts.[6−9] A bimetallic system of Pt on Pd can produce a small strain, allowing the weak lattice contraction to produce a downshift of the d-band center and decreasing the binding strength of the adsorbed intermediates.[10,11]

However, the durability of catalysts must be improved for it to be useful in actual fuel cell devices. There have been reports of Pd dissolution under fuel cell operating conditions, in which the dissolved Pd ions affected the cell's performance.[12] However, the predominant mechanisms of electrode degradation include the dissolution of Pt and the growth of Pt particles, oxidation of the carbon support and the dissolution of metal from Pt metal alloy catalysts. Ostwald ripening and coalescence have been suggested as Pt degradation mechanisms.[13−15] During PEMFC operations, physically and electrochemically harsh conditions, such as high potentials, high temperatures, low pH values, and increased humidity, promote particle

Received: April 15, 2015
Accepted: June 10, 2015
Published: June 10, 2015

DOI: 10.1021/acsami.5b03255
ACS Appl. Mater. Interfaces 2015, 7, 14053−14063

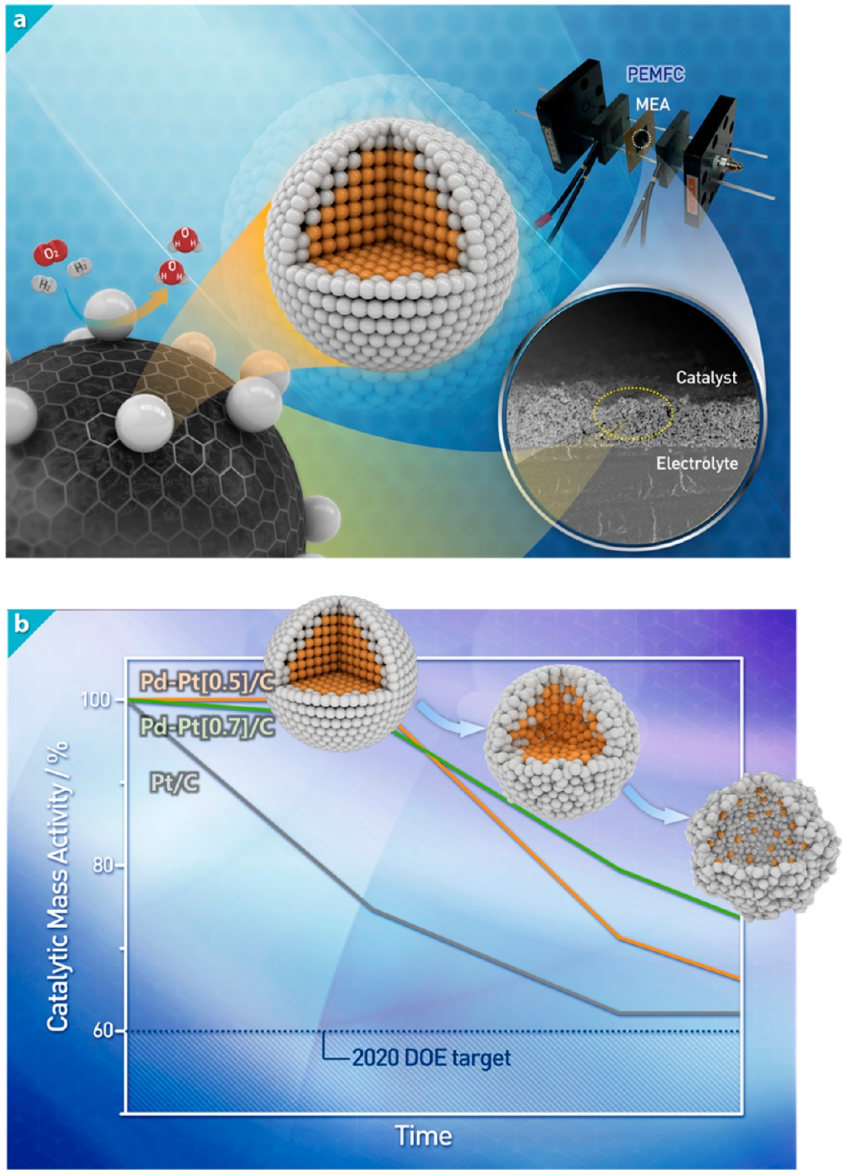

Figure 1. Conceptual diagrams of Pt-exoskeleton catalyst-based MEA and durability properties; (a) Pt-exoskeleton catalyst-based MEA and single cell. Inset FE-SEM image is cross-section of Pt-exoskeleton catalyst-based MEA; (b) durability properties and degradation process of Pd–Pt/C catalyst during ADT.

growth. Yet, the primary reason for the reported degradation of Pt metal alloy catalysts is the dissolution of a secondary metal in the acid media, which decreases cell performance.[16] Gasteiger et al. have investigated the mechanism of base metal loss in Pt metal alloy catalysts. These authors presented possible explanations for the leaching of the base metal from Pt metal alloy catalysts in PEMFCs, including the presence of excess base metal, incomplete alloying and a thermodynamically unstable base metal.[17] Nevertheless, it is well-known that core–shell nanoparticles with Pt monolayers exhibit significantly enhanced mass activity and specific activity because the core metal induces a reduction in the Pt mass and a change in Pt surface structures. Sasaki et al. have reported high stability for Pd–Pt monolayer shell electrocatalysts in an accelerated degradation tests (ADT) with 100 000 potential cycles.[18] The electrocatalysts exhibited small losses of electrochemical surface area (ECSA) and activity and a negligible loss of Pt. Chen et al. have investigated the effect of Pt shell coverage for Ni–Pt core–shell nanoparticles and concluded that increasing the Pt content increased neither the ORR activity nor the durability of the catalyst.[19] However, Choi et al. have reported that electrocatalysts with thin Pt shells (Pd:Pt = 1:0.5 and 1:1.0) are less stable than those with thick Pt shells (Pd:Pt = 1:1.5) during harsh potential cycling.[20] Sasaki and Choi independently studied the same materials and obtained different results. Therefore, there are insufficient data from which to conclude whether core–shell catalysts can actually replace commercial Pt/C catalysts in fuel cells. Almost all of the studies on core–shell structure catalysts have used half-cells and are therefore not representative of real PEMFC operation conditions.

However, it can be challenging to perform conclusive and practical studies on the durability of Pd–Pt bimetallic catalysts under real PEMFC conditions because of the prolonged test period and the complexity of the failure analysis. Therefore, ADTs have been developed as a valuable tool for investigating mechanisms of degradation. The parameters in ADTs include

DOI: 10.1021/acsami.5b03255
ACS Appl. Mater. Interfaces 2015, 7, 14053–14063

the potential cycle numbers, current density, potential, operating time, cell operating conditions, gas permeability, and other component conditions.[21−23] Gasteiger et al. has stated that the potential cycling test is more relevant to the actual drive cycle of PEMFCs in vehicles than are constant current or constant potential tests.[23] The degradation of cell performance is more severe in a potential cycling test than in the constant current or constant potential tests. Additionally, the load-cycling test, which involves various severe conditions, including a high current density (low cathode potential), a low current density (high cathode potential), and a holding period at the OCV, is a harsher test than the other modes.

In this study, we synthesized Pd-metal-based Pt-exoskeleton catalysts with high stability and remarkable activity, and demonstrated the outstanding performance of these materials when used in membrane-electrode assemblies (MEAs, Figure 1) in a PEMFC single cell. The primary objective of this study was to investigate the performance of Pt-exoskeleton catalysts in an MEA in a single cell rather than to explore a novel synthesis for core−shell structure or the high activity that can be achieved using a half-cell. Furthermore, the performance degradation of Pt-exoskeleton catalysts in an MEA was investigated using a continuous load-cycling test on a single cell. The operating conditions using single cell, including high temperature, low pH, actual pressure, and fuel flows, are more relevant to the real performance of a fuel cell system than those of a half-cell condition or potential cycling. To determine the durability and tendency toward degradation of the bimetallic catalysts, we conducted electrochemical and structural analyses on MEAs with the catalysts before and after the ADT.

2. EXPERIMENTAL SECTION

2.1. Structural Analysis. The Pd-metal-based Pt-exoskeleton nanoparticles are referred to as Pd−Pt/C hereafter, more specifically, for Pd−Pt[*n*]/C, where *n* is the atomic ratio of Pt (Pd:Pt = 1:*n*). X-ray diffraction (XRD) analysis was carried out to investigate the change in the crystallite sizes of Pt/C, Pd−Pt[0.5]/C, and Pd−Pt[0.7]/C before and after the ADT. The XRD measurements were carried out using a Rigaku D/MAX 2500 with a Cu*Kα* source (λ = 1.541 Å) at 40 kV and 100 mA. The samples were scanned from 20 to 80° at 2° min^{-1}. The valence state and composition of Pd−Pt[0.5]/C and Pd−Pt[0.7]/C after the ADT were determined using X-ray photoelectron spectroscopy (XPS) with an ultrahigh vacuum (UHV) multipurpose surface analysis system (SIGMA PROBE, Thermo, UK) that operated at base pressures <1 × 10^{-10} mbar. The photoelectron spectra was excited using an Al K*α* (1486.6 eV) anode operating at a constant power of 100 W (15 kV and 10 mA). During acquisition of the spectra, a constant analyzer energy (CAE) mode was employed at a pass energy of 40 eV and a step of 0.1 eV. The electron binding energy scale was calibrated from the hydrocarbon contamination observed in the C 1*s* peak at 284.6 eV. The core peaks were analyzed using a nonlinear Shirley-type background, and the peak position and area were obtained by weighted least-squares fits of model curves (70% Gaussian, 30% Lorentzian) to the experimental data. The structures of the cross sections of the Pt/C MEA, Pd−Pt[0.5], and Pd−Pt[0.7]/MEA before and after the ADT were examined using field emission-scanning electron microscopy (FE-SEM, JSM 6700F, JEOL Ltd.) to confirm the morphological changes of the electrodes and the connection between the catalyst layer and the membrane. The chemical composition and the distribution of various elements of the MEA before and after the ADT were evaluated using energy-dispersive X-ray (EDX; 7421, OXFORD) combined with FE-SEM.

2.2. Electrochemical Analysis. The single-cell performance was measured for each MEA, which had a geometric area of 5 cm^2. An MEA was placed between two gas diffusion layers (GDLs, E-TEK) and inserted into graphite plates containing serpentine flow channels. The single cell was assembled using a torque wrench to match the pressure applied at the moment of setting the cell. Figure 2.2 is a photograph of the single cell that was used in this study. The single cell was connected to a fuel cell test station (FCTS, WonATech Co., Ltd.). To carry out performance measurements, humidified H_2 and air were fed to the anode and cathode at a stoichiometric ratio of 1.5/2 and temperature of 75/70 °C. The cell temperature was set at 70 °C, and the backpressure on the cell was the ambient pressure. The cell voltage of each MEA was obtained by increasing the current density using a fuel cell test station to generate current−voltage curves by the current sweep method at a 10 mA cm^{-2} s^{-1} rate.

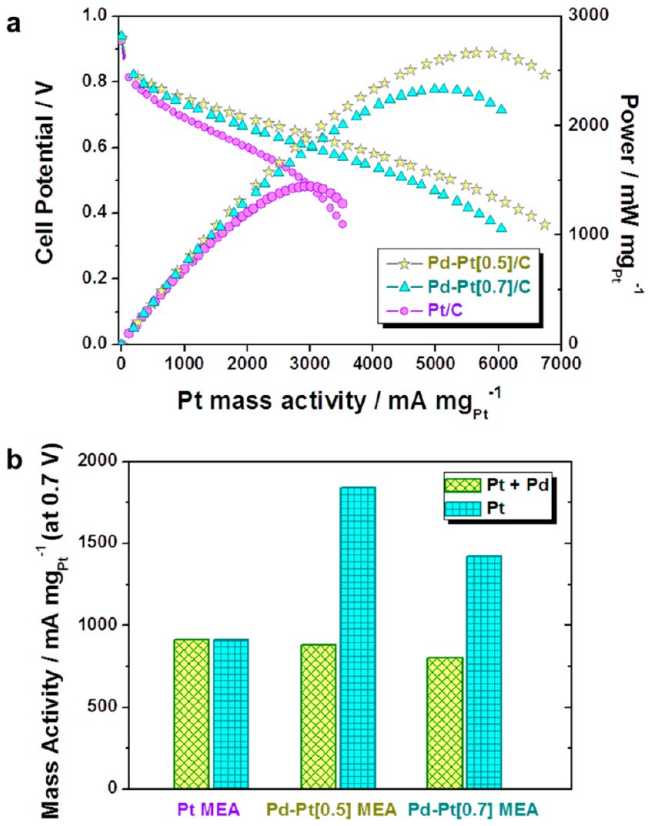

Figure 2. Pt mass activity from IVP for Pt-exoskeleton catalyst-based MEAs; (a) polarization curves for each MEA; the cell voltages were obtained by increasing the current density and using a fuel cell test station to measure the current−voltage curves; the test was performed at 70 °C; fully humidified H_2/air was used in the MEA under atmospheric pressure; (b) comparison of Pt mass activity at 0.7 V; currents were normalized to the Pt loading amount.

2.3. Fabrication of MEAs. The catalyst inks for the cathode were fabricated ultrasonically using the synthesized Pd−Pt/C core−shell catalysts and a commercial Pt/C catalyst with a 5 wt % Nafion solution (Aldrich Chem. Co.) in D.I. water and isopropyl alcohol (IPA, Aldrich Chem. Co.) as the solvent. The carbon-supported Pt catalyst powder (40 wt % Pt/C, Johnson Matthey, mean diameter ∼3.0 nm)as used as the catalyst for the anode. The anode catalyst inks were prepared using the aforementioned method. The Nafion 212 membrane was pretreated with a hydroperoxide solution (3 wt %) for 1 h and a sulfuric acid solution (0.5 M) for 1 h at 100 °C. The pretreated membrane was dried and placed in the appropriate frame. To prepare the MEAs, we sprayed the catalyst inks directly onto both sides of the pretreated Nafion 212 membrane to form the catalyst-coated membrane (CCM). The metal catalyst was loaded at 0.2 and 0.3 mg cm^{-2} on the anode and cathode electrodes, respectively. The active surface area of the MEA was 5 cm^2. Pt/C, Pd−Pt[0.5]/C, and Pd−Pt[0.7]/C catalysts were used as cathode catalysts in the MEAs.

DOI: 10.1021/acsami.5b03255
ACS Appl. Mater. Interfaces 2015, 7, 14053−14063

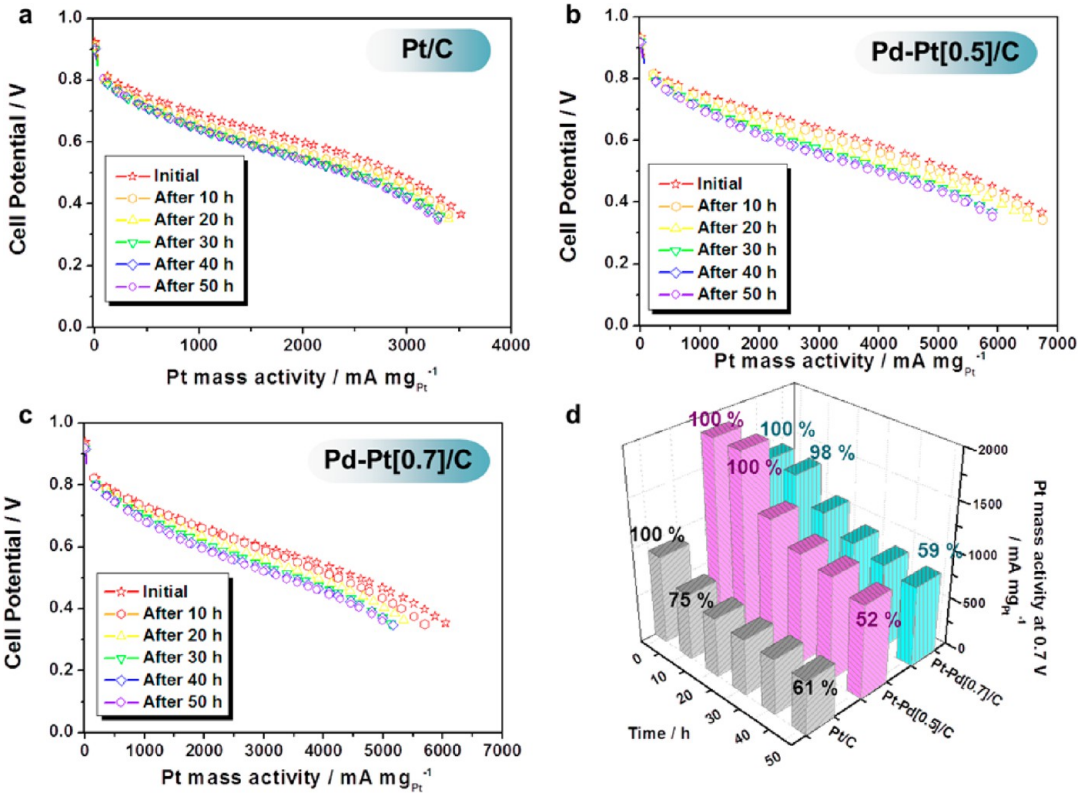

Figure 3. Polarization curves at specified time intervals during ADT; (a) commercial Pt/C-based MEA; (b) Pd−Pt[0.5]-based MEA; (c) Pd−Pt[0.7]-catalyst-based MEA; (d) changes in Pt mass activity of the MEAs with Pt/C, Pd−Pt[0.5]/C and Pd−Pt[0.7]/C cathode catalysts at specified time intervals (after 10, 20, 30, 40, and 50 h of operation) at 0.7 V; the ADT comprised load cycling between 0.35 and the OCV with a 30 s dwell time at 70 °C, with the single cell continuously connected to the fuel cell test station during the test.

2.4. ADT for a Single Cell. The performance degradation of the MEAs with Pt/C, Pd−Pt[0.5]/C, and Pd−Pt[0.7]/C as cathode catalysts were investigated by performing ADTs on the prepared MEA for 50 h. The ADT was carried out using repeated load cycling, which entailed increasing the cell current at 50 mA s^{-1} from the OCV to 0.35 V, shutting off the load and then maintaining the OCV for 30 s. The operating conditions of the ADT were the same as those used during the current−voltage characterization. Cyclic voltammetry (CV) was carried out to estimate the electrochemical surface area (ESA) of each MEA before and after the ADT. CV was performed over a scan range from 0.00 to 0.95 V at a scan rate of 100 mV s^{-1}. Humidified H_2 was fed into the anode as the reference electrode, and humidified N_2 was fed into the cathode as the working electrode. High resolution-transmission electron microscopy (HR-TEM) was conducted to observe changes in the morphology, particle size, and size distribution of the Pt/C, Pd−Pt[0.5]/C, and Pd−Pt[0.7]/C nanoparticles before and after the ADT. The samples were prepared by scraping the catalyst layer to peel off the catalysts from the MEA and then suspending the catalysts in ethanol. The samples were dropped onto a carbon film that was supported on a copper grid, and the solvent was evaporated off. The HR-TEM images were obtained using a JEOL 2010 at a 200 kV accelerating voltage.

3. RESULTS AND DISCUSSION

3.1. Single-Cell Performance in the ADT. Carbon-supported bimetallic catalysts were prepared using a hydroquinone reduction method, as described in our previous study.[24] The core base metal was Pd and the exoskeleton metal was Pt. The catalyst inks for the cathode were fabricated using the developed Pd−Pt/C catalysts, and a commercial Pt/C catalyst. To fabricate the MEAs, we sprayed the catalyst inks directly onto both sides of a pretreated Nafion 212 membrane to form a catalyst-coated membrane (CCM).[25] The commercial Pt/C catalyst-based-MEA will be referred to as Pt/C MEA and Pd−Pt[n]/C catalyst-based-MEA will be referred to as Pd−Pt[n]/C MEA. The half-cell activities of the Pd−Pt/C catalysts (Figure S1 in the Supporting Information) clearly demonstrated that the particles had good catalytic activity for ORR that was comparable to that of commercial Pt/C.[24] In addition, the Pd−Pt/C catalysts performed remarkably well in a practical PEMFC device, i.e., an MEA in a single cell (Figure 2). Figure 2a presents the initial performance of the MEAs. The current densities were normalized to the loading amount of Pt, i.e., the currents of Pd−Pt[0.5]/C and Pd−Pt[0.7]/C were multiplied by the wt % ratio of Pt (100/47.82 and 100/56.2, respectively). Cell performance was compared at 0.7 V because activation kinetics were dominant in the low current region (Figure 2b). Figure S2 in the Supporting Information presents the polarization curves, which were normalized to the active area, and the metal price. All of the results indicated that the catalytic activity of the Pd−Pt/C catalysts was comparable to that of the commercial Pt/C at the same Pt loading (by factors of 2.04 and 1.56). For a relatively thin Pt-exoskeleton (or shell; the shell used in this study was a few atomic layers thick; see the Supplementary Information for details on the Pt shell thickness), electronic coupling between the Pd core and the Pt shell may enhance cell performance. Combining Pt with Pd has also been found to significantly affect the electronic structures of Pt, and therefore its catalytic properties for specific reactions, through the formation of Pd−Pt bonds. For a bimetallic catalyst made of Pt on Pd, a small compressive strain originating from weak lattice contraction causes a downshift of

DOI: 10.1021/acsami.5b03255
ACS Appl. Mater. Interfaces 2015, 7, 14053−14063

Table 1. Electrochemical and Physical Properties of Commercial Pt/C and Pt-Exoskeleton Catalyst-Based MEAs before and after ADT

category	properties		Pt/C		Pd−Pt[0.5]/C		Pd−Pt[0.7]/C	
			before	after	before	after	before	after
electro-chemical properties	ECSA ($m^2\ g^{-1}$)		33.1	26.9	24.3	23.0	29.6	28.3
	R_Ω ($\Omega\ cm^2$)		0.07	0.07	0.07	0.08	0.07	0.08
	R_C ($\Omega\ cm^2$)		0.17	0.16	0.19	0.24	0.18	0.26
	OCV (V)		0.922	0.897	0.934	0.918	0.939	0.919
	Pt activity (mA mg_{Pt}^{-1})	at 0.8 V	160	90	381	188	320	146
		at 0.7 V	910	552	1853	966	1423	836
		at 0.6 V	2000	1390	3680	2221	3025	1886
		at 0.5 V	2860	2408	5270	3940	4591	3317
physical properties	mean particle size from TEM (nm)		3.38	4.94	4.04	4.91	4.37	4.73
	mean crystallite size from XRD (nm)		3.76	5.01	3.98	4.99	4.30	4.71
	(220) peak position (deg)		67.46	67.60	67.66	67.93	67.60	67.76
	Pd atomic composition (at. %)	from EDX			66.87	50.29	62.80	52.45
		from XPS			43.82	39.19	35.13	33.71
	Pt atomic composition (at. %)	from EDX			33.13	49.72	37.20	47.55
		from XPS			56.18	66.81	64.88	66.29

the d-band center, thereby reducing the binding strength of the adsorbed intermediates. This behavior can reduce or improve catalytic activity, depending on whether adsorption or desorption of the intermediates limits the reaction rate.[7,10,11] That is, the outstanding performance of the Pd−Pt/C catalysts based on an MEA can be explained in terms of electronic structures and the d-band center.

Figure 3 and Figure S3 in the Supporting Information show the polarization curves of Pt/C, Pd−Pt[0.5]/C, and Pd−Pt[0.7]/C MEA at specified time intervals under load cycling. The ADT involved load cycling, which consisted of increasing the cell current at 50 mA s^{-1} from the OCV to 0.35 V, shutting off the load and then maintaining the OCV for a 30 s dwell time at 70 °C. The performance of the initial MEA was approximately 910 mA mg_{Pt}^{-1} at 0.7 V, whereas the corresponding performance after operating for 50 h was approximately 550 mA mg_{Pt}^{-1} for the Pt/C MEA (Figure 3a). The performance decrease ratio was approximately 39%; it should be noted that the decrease in the performance was only significant during early operation (0−10 h) and became less prominent after 10 h of operation. Figure 3d shows the behavior of the Pt mass activity versus time for the ADT at 0.7 V. The decrement rate of Pt indicates that the crucial decay in Pt/C MEA occurred during the initial period of 0−10 h. The degradation in single cell performance could be categorized into recoverable and unrecoverable degradation processes.[26−31] For the Pt/C MEA, the unrecoverable degradation process affected the initial rapid decrease in performance. The sintering and aggregation of the catalyst particles and the loss of ECSA were confirmed, which will be discussed later and are summarized in Table 1.

Figure 3b, c shows that superior performance was obtained using the MEA with a Pd−Pt/C cathode catalysts even though the catalyst ink conditions (e.g., the ionomer and solvent ratios) of the MEAs were optimized to correspond to a commercial 40 wt % Pt/C catalyst. The decrement rates of Pd−Pt[0.5] and Pd−Pt[0.7]/C MEA were approximately 48 and 41%, respectively. Figure 3d shows that during early stages of the ADT (from 0 to 10 h), the decrement rates of Pd−Pt[0.5]/C and Pd−Pt[0.7]/C MEAs were approximately 2%; using Pd−Pt[0.5]/C resulted in nearly identical performance with a much smaller ratio than that of Pt/C. However, the performance of the Pd−Pt/C catalysts dramatically decreased from 10−50 h, whereas the Pt/C catalyst performed steadily up to the end of the ADT after an initial rapid decay. The decrement rate of Pd−Pt[0.5]/C was higher than that of Pd−Pt[0.7]/C throughout the entire regime. This decline in the performance of the Pt/C and Pd−Pt/C MEAs indicated that distinct mechanisms controlled the degradation of Pt/C and Pd−Pt/C catalysts. Therefore, the Pd base metal in Pd−Pt/C catalyst nanoparticles may perform stably during an initial operation period, but it does not remain stable for more than 10 h. These results are rationalized by the leaching of base metal Pd (discussed later).

3.2. Structural and Electrochemical Analyses. A FE-SEM analysis was performed before and after the ADT to investigate structural changes in the MEA structure and determine the source of degradation after the ADT (Figure 4 and Figure S4 in the Supporting Information). Other studies have reported degradation of the MEA structure after an ADT; for example, mechanical stresses, such as nonuniform contact pressure, and fatigue from stresses induced by temperature and humidity can cause thinning of the membrane and cracks in the catalyst layer. The catalyst layer was also thinned because of carbon corrosion within the layer. These changes in the MEA structure diminished cell performance because of an increase in the contact resistance and hydrogen crossover. However, in this study, no significant changes were observed in the MEA structure in any of the cases considered. A few metal islands were observed for the Pd−Pt/C MEAs after the ADT, as shown in the SEM images in Figure 4. For the Pt-metal bimetallic catalysts, both Pt and the nonprecious metal particles dissolved during fuel cell operation. The dissolved Pt was redeposited on the surface of the catalyst particles, whereas the dissolved nonprecious metal ions diffused into the membrane, were reduced and formed metal islands inside the electrolyte membrane. The element in the metal islands inside the membrane was confirmed by performing energy dispersive X-ray analysis (EDX). A band of elemental Pd appeared inside the membrane, whereas no significant signal was observed from the Pt/C MEA. This result indicated that the Pd in the Pt-exoskeleton catalyst may have dissolved and diffused into the membrane, unlike the Pt. This dissolution of the secondary metal and increase in the residual particle size may have caused

DOI: 10.1021/acsami.5b03255
ACS Appl. Mater. Interfaces 2015, 7, 14053−14063

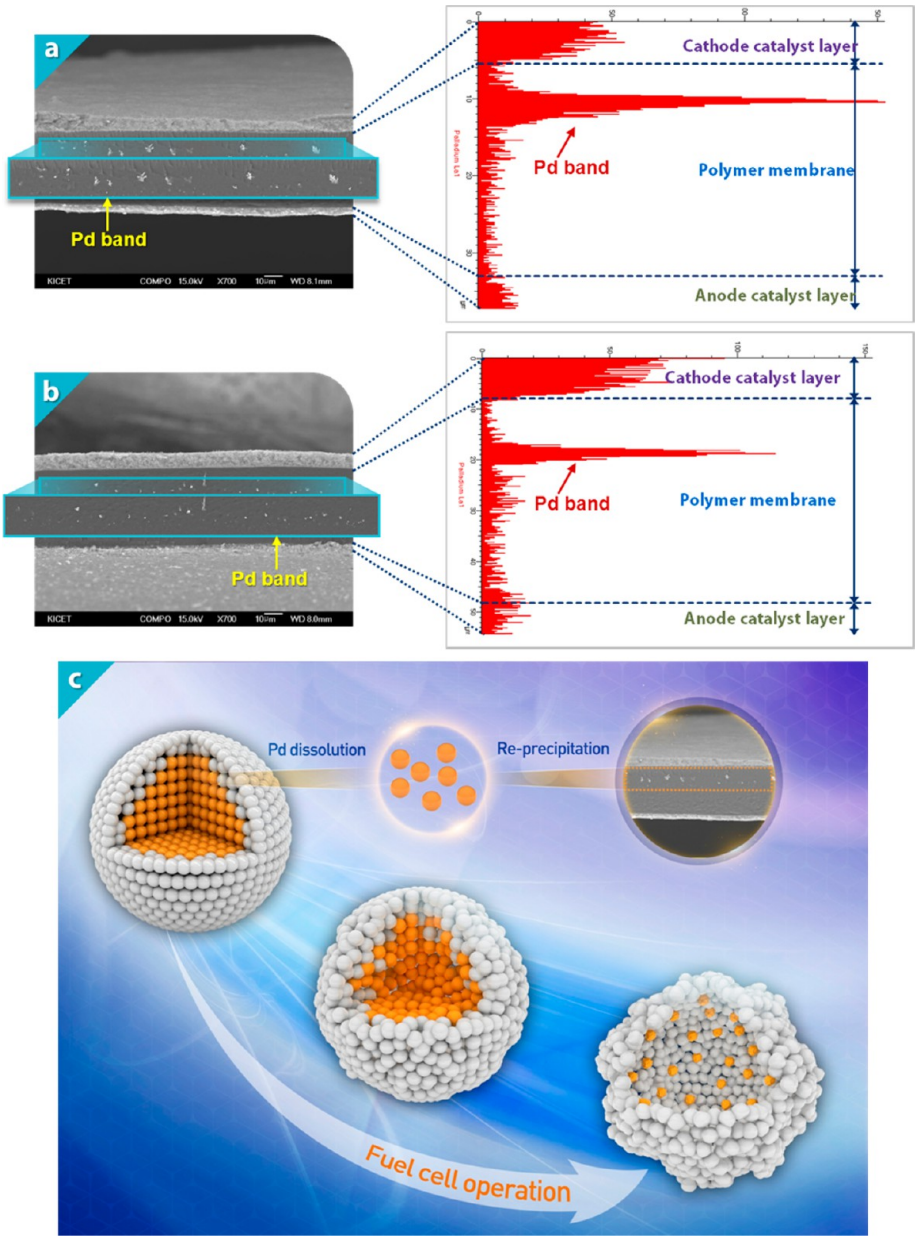

Figure 4. FE-SEM cross-section images of MEAs after ADT and the corresponding elemental distribution of MEAs after ADT; (a) Pd–Pt[0.5]/C and (b) Pd–Pt[0.7]/C, (c) conceptual diagrams of degradation process of Pd–Pt/C catalyst during ADT.

the observed decrease in performance. Pd dissolution occurs at a potential of 0.92 V, which is lower than the corresponding potential for Pt (1.19 V). Pd is therefore more reactive than Pt and has a lower standard electrochemical potential. Furthermore, the Pd in the Pd–Pt/C may have dissolved to form Pd^{2+}, allowing the Pd ion to diffuse through the imperfection in the Pt shell during the ADT and precipitate inside the membrane. This precipitation formed the Pd band shown in Figure 4. This result is similar to the Pt band that forms on a Pt/C MEA following the dissolution of Pt during an ADT.[17] Adzic and coworkers have reported that placing a Pt monolayer on a Pd substrate shifted the relative dissolution potential, and the partial dissolution of Pd increased the core–shell interaction.[18]

The elemental composition of the catalyst layer before and after ADT was characterized using energy EDX (Figure S5 in the Supporting Information). The initial Pd atomic ratios in Pd–Pt[0.5] and Pd–Pt[0.7] decreased after the ADT. This result also indicated strong dissolution of Pd in the Pd–Pt/C during the ADT. Changes in the atomic ratio indicated that Pd–Pt[0.7]/C was more stable than Pd–Pt[0.5]/C. Table 1 shows the bulk metal atomic ratios that were determined using EDX.

The difference between the ECSA values of the Pt/C MEA and the Pd–Pt/C MEAs before and after the ADT were determined using cyclic voltammetry (CV) (Figure 5). The shape of the CV curve for Pd–Pt[0.5] was similar to that of Pd–Pt[0.7]. Figure 5 shows well-defined hydrogen adsorption/desorption peaks and oxidation/reduction peaks. The HUPD regions of the Pd–Pt/C MEA exhibited relatively broader peaks than those of the Pt/C MEA because of changes in the surface geometry caused by the interaction between the Pd core and the Pt layer.[20] The ECSA in the present study tends to be lower than others in the literature, but a direct comparison of

DOI: 10.1021/acsami.5b03255
ACS Appl. Mater. Interfaces 2015, 7, 14053–14063

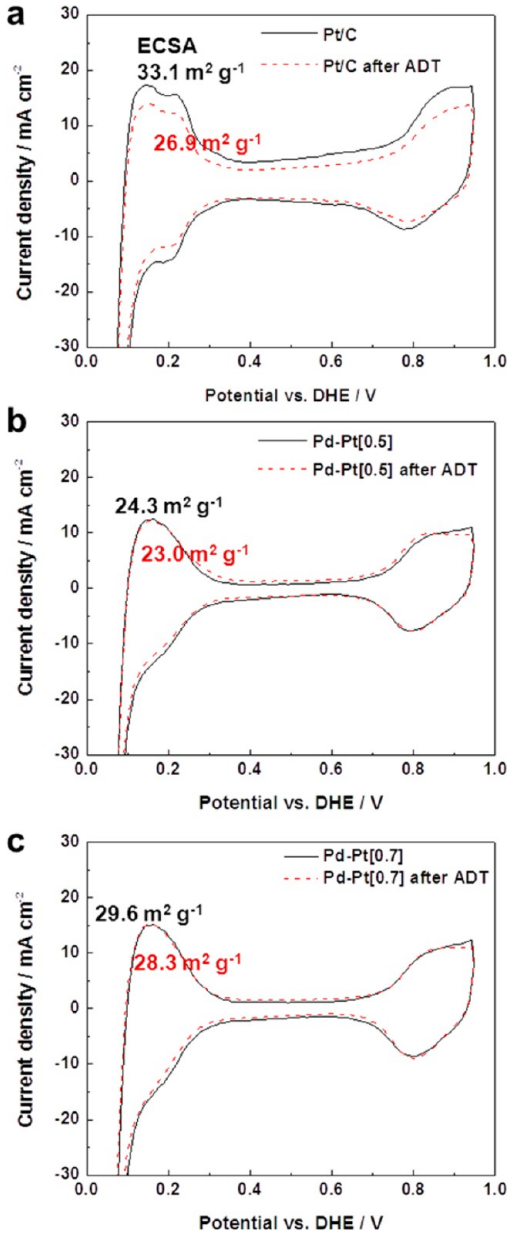

Figure 5. Cyclic voltammograms of Pt/C, Pd−Pt[0.5]/C and Pd−Pt[0.7]/C before and after ADT; (a) commercial Pt/C-based MEA; (b) Pd−Pt[0.5]-catalyst-based MEA; (c) Pd−Pt[0.7]-catalyst-based MEA; ECSA was calculated from hydrogen adsorption/desorption peaks and is shown for comparison.

these results is not possible because of differences between the main objectives and experimental conditions of the studies.

The ECSAs of the samples measured using CV are given in Table 1. The reduced rates of the Pt/C MEA, Pd−Pt[0.5]/C MEA, and Pd−Pt[0.7]/C MEA were 18.7, 5.3, and 4.4%, respectively. These CV results suggested that the reduced performance of Pt/C MEA was associated with the loss of ECSA. As reported in previous studies, the ECSA of Pt/C MEA was significantly reduced after the ADT.[30,31] However, the rate of decrease of the ECSA was negligible in the Pd−Pt/C MEAs. These results suggest that decreased performance of the MEA with the Pd−Pt/C catalysts was not associated with ECSA loss. In response to these findings, a further HR-TEM analysis of the MEAs was conducted after the ADT (Figure 6). Figure 6a, d shows the results for Pt/C before and after 50 h of ADT. A mean particle size of approximately 4.94 nm was measured independently from 100 nanoparticles in the TEM images. The Pt particle size increased from 3.83 to 4.94 nm after 50 h of ADT. Certain particle agglomerates were found in the HR-TEM images but not observed in fresh Pt (Figure 6a). The increase in the Pt particle size affected the ECSA loss measured using CV, as shown in Figure 5. Wilson et al. hypothesized that the Pt particle size in aged MEA increased because of crystallite migration during gas phase sintering. The increase in particle size corresponded to the loss of active surface area.[9] However, in many studies, the dissolution and redeposition of Pt have been proposed as the primary mechanisms of degradation for the Pt electrocatalyst in a fuel cell system, and Pt dissolution has been found to increase with the potential in the 0.85−0.95 V range.[13,15] In this study, an ADT was performed in the range from 0.35 to the OCV (>0.9 V), and the operating conditions were similar to those used in other studies. The most significant migration of Pt has been reported to occur on the cathode side of the MEA after potential cycling to the OCV or higher voltages.[28] These ADT operating conditions might correspond to an increase in the Pt particle size. Figure 6e, f shows the HR-TEM images of Pd−Pt/C after the ADT. The mean particle sizes of Pd−Pt[0.5] and Pd−Pt[0.7] were approximately 4.91 and 4.73 nm, respectively. The rate of increase for the mean particle size was lower than that for the Pt. For the Pt metal alloy catalysts, both Pt and the nonprecious metal particles could be dissolved. Popov and co-workers suggested that the primary cause for decay in the catalytic activity of the Pt metal alloy catalyst was ECSA loss due to metal dissolution.[16,17] However, such core−shell structure catalysts exhibited distinct trends in performance degradation and ECSA compare with those of the Pt metal alloy. The shapes of the CV and ECSA curves for the Pd−Pt/C catalysts were close to similar before and after ADT, whereas the corresponding curves for the existing Pt metal alloy catalysts were clearly different. This result indicates that the primary cause of degradation in the Pd−Pt/C catalysts was not the loss of ECSA. The loss of ECSA was negligible in these catalysts. Sasaki et al. have suggested that the hollow structures that can form under potential step cycling (from 0.7 to 0.9 V) should have the highest dissolution potentials for Pd core/Pt monolayer shell electrocatalysts. Core−shell catalysts have been reported to show a small loss of ECSA and catalytic activity after 1 000 000 cycles.[18] However, although the loss of ECSA was negligible in this study, as was observed in Sasaki's study, the stability was significantly reduced. The Pd component of the Pd−Pt/C catalysts dissolved under the high potential and diffused through imperfections in the Pt shell during the ADT. Consequently, the remaining Pt in the Pd−Pt/C catalysts formed a partially hollow structure.[32,33] In addition, a portion of the Pd may have participated in hydrogen adsorption/desorption. Therefore, although the particle size increased, the ECSA level remained nearly constant. ECSA is a general indicator of the capacity of a catalyst for hydrogen adsorption/desorption because the ECSA depends on the exposed Pt surface area and structure. Moreover, nanometer-sized Pd−Pt/C materials are not stable under real PEMFC conditions and suffer compositional/structural changes due to interparticle and intraparticle movements of metal atom/species.[32] These phenomena strongly diminished the catalytic activity of the Pt-exoskeleton catalysts.

The primary reason for the degradation of the Pt/C MEA again appeared to be the dissolution and growth of Pt particles

DOI: 10.1021/acsami.5b03255
ACS Appl. Mater. Interfaces 2015, 7, 14053−14063

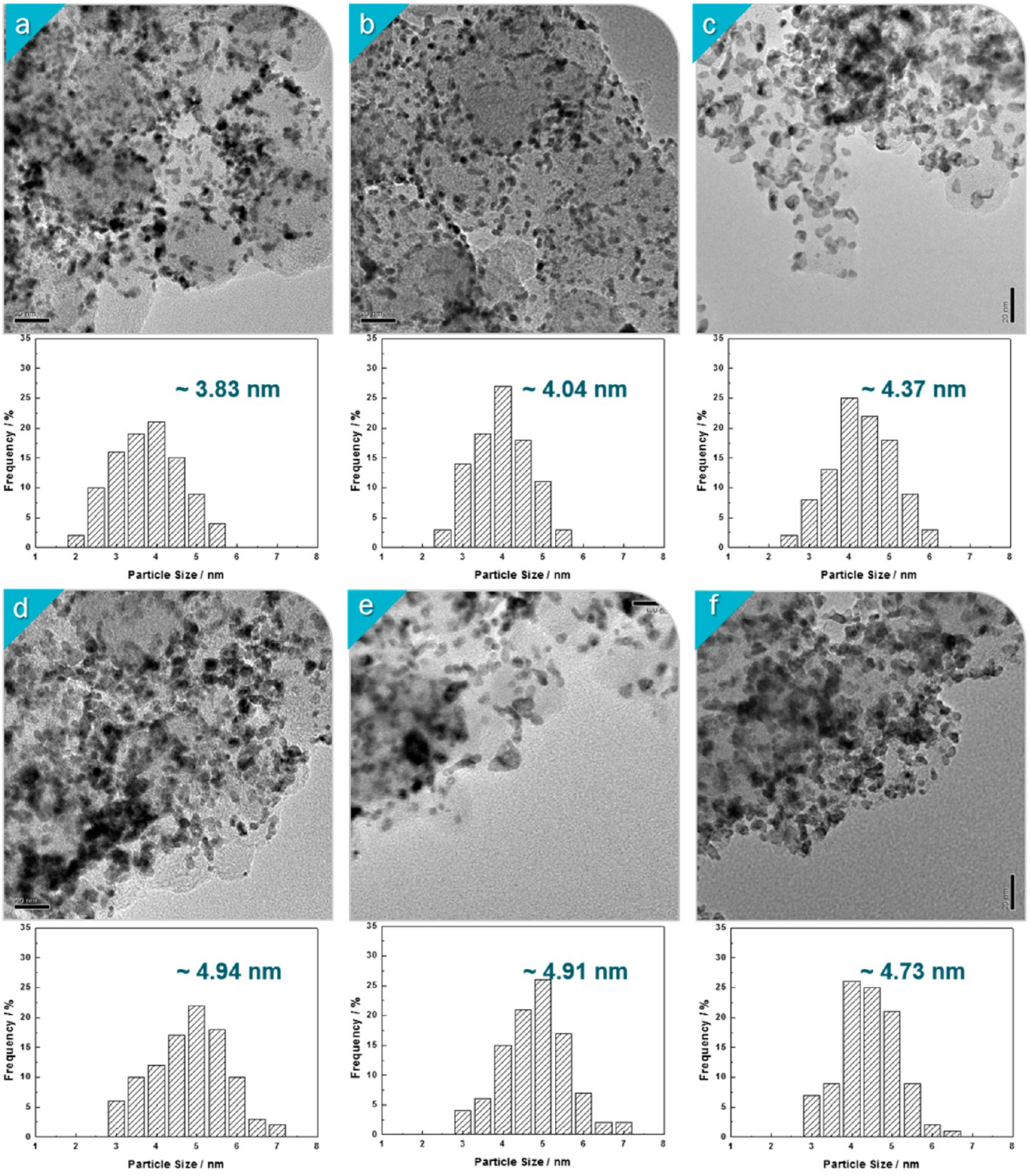

Figure 6. TEM images of Pt/C, Pd−Pt[0.5]/C and Pd−Pt[0.7]/C catalysts before and after ADT; (a, d) initial Pt/C and after ADT; (b, e), initial Pd−Pt[0.5]/C and after ADT; (c, f) Pd−Pt[0.7]/C and after ADT; the bottom shows size distribution histograms.

accompanied by the loss of ECSA throughout the entire ADT period. However, the Pd−Pt/C MEA exhibited enhanced durability during the early stages of the ADT (approximately 10 h). The Pd component in the core stabilized the Pt exoskeleton by positively shifting its oxidation potential and preventing the cathode potential from reaching values at which Pt dissolution would occur.[18] An intact shell is an important factor in stability and activity, but it is difficult to synthesize a fault-free core−shell nanoparticle in practice. If the core Pd particles (which were 3.76 nm in our case) were completely covered with a monatomic layer of Pt, the layer thickness would then have been equivalent to the diameter of a Pt atom (0.36 nm, considering adsorbed anions),[34] and the atomic ratio Pt between Pd should have been approximately 0.3 (details provided in the Supporting Information). However, the atomic ratios for Pt and Pd were 0.5 and 0.7, respectively. Therefore, it is possible that there were defects or extra Pt on the Pd surface. There were certainly partial punctures or incomplete alloying of

DOI: 10.1021/acsami.5b03255
ACS Appl. Mater. Interfaces 2015, 7, 14053−14063

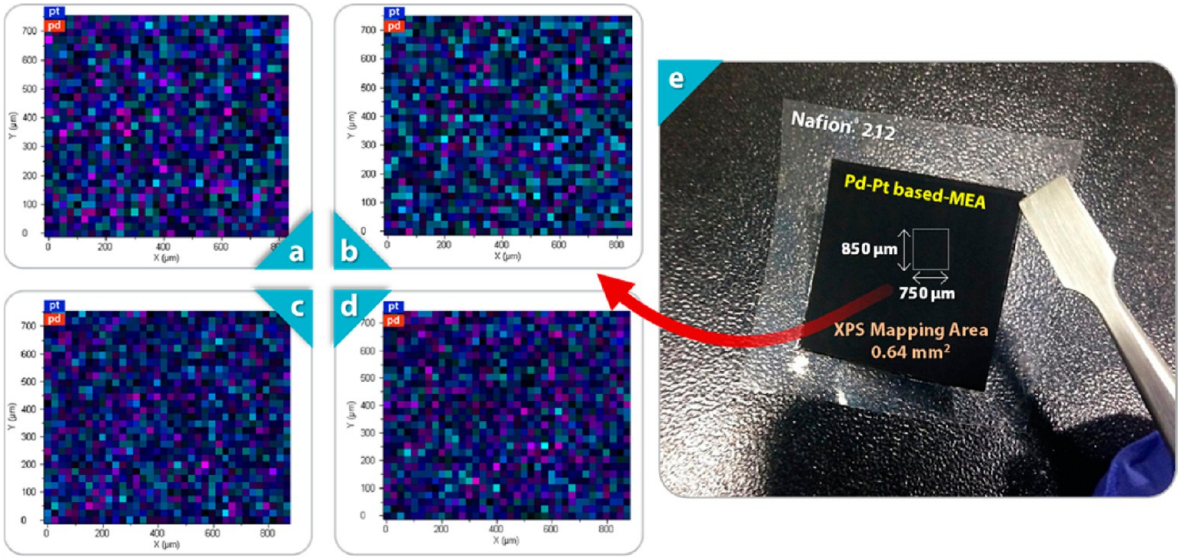

Figure 7. XPS element mapping images of MEAs before and after ADT; (a) Pd−Pt[0.5]-catalyst-based MEA before ADT and (b) after ADT; (c) Pd−Pt[0.7]-catalyst-based MEA before ADT and(d) after ADT; (e) photograph of surface of Pd−Pt catalyst-based MEA.

the core−shell structure; hence, significant oxidization and dissolution of Pd could have occurred through contact with the electrolyte during the prolonged potential cycling when the dissolution potential was reached. The dissolved Pd^{2+} was then reduced by H_2 diffusing from anode and redeposited on the membrane; these Pd particles may have decreased the membrane stability and hindered reactant transport during the late stages of the ADT (20−50 h). The loss of ECSA was negligible at this time, but the stability was notably reduced, as in this study.

These phenomena were further investigated by performing X-ray diffraction (XRD) analysis on a filmlike CCM state. Figure S6 in the Supporting Information shows the XRD patterns of the catalysts before and after the ADT, and the catalyst properties are summarized in Table 1. The dashed line represents the peak position of the initial Pt. It is well-known that Pt and Pd have typical fcc lattice structures with intrinsic peaks corresponding to the (111), (200), and (220) planes and similar atomic sizes and crystal structures. In all of the cases investigated, the XRD profiles of the Pd−Pt/C catalysts exhibited the primary peaks of an fcc structure. The (220) peak was used to calculate the average particle size of the catalysts using the Scherrer equation because the (111) and (200) peaks overlapped the broad C peaks. As expected, the mean crystallite size of Pt/C increased from 3.76 to 5.01 nm after the ADT, which was in good agreement with the results of the HR-TEM analysis. The increase in the mean crystallite size of Pt corresponded to the loss of ECSA according to CV. The size of the Pd−Pt[0.7]/C catalyst only increased by 0.4 nm, whereas that of the Pd−Pt[0.5]/C catalyst increased by 1.0 nm. This result could be attributed to the thinner Pt shells being more exposed to dissolution and redeposition during harsh potential cycling. In addition, the (220) peaks of Pd−Pt[0.5] and Pd−Pt[0.7] were shifted to higher theta positions, and their shapes were asymmetric (Figure S6 in the Supporting Information and Table 1). This result indicated that the Pd−Pt/C partially collapsed during the ADT and that the Pd−Pt[0.5]/C catalyst decayed further than did the Pd−Pt[0.7]/C catalyst. Diffraction peak shifts and asymmetries are generally owing to strain, lattice defects and dislocations of the Pd−Pt/C catalysts and chemical heterogeneities can cause peak broadening. Dissolved Pd metal in Pd−Pt/C catalysts leave the surface of the catalyst Pt-rich and separate from core−shell structure, hence the structure was collapsed and caused a peak shifts and asymmetries. Overall, the amount of deposited Pt shell on Pd core affected the degradation of the core−shell catalyst.[20] Choi et al. reported ORR electrocatalytic performance as a function of the shell thickness. The ORR performance was highly dependent on the Pt shell thickness, and even Pd−Pt[0.5]/C exhibited high mass activity; however, considering both activity and durability, the Pd−Pt[0.7] was the more promising ORR electrocatalyst.

The chemical composition of the MEA electrode surface was determined using X-ray photoelectron spectroscopy (XPS) (details provided in Figure S7 and the note in the Supporting Information and Table 1). The peak intensity of Pd decreased after the ADT because of Pd dissolution, and the change in the atomic ratio revealed that Pd dissolution occurred in the Pd−Pt/C catalysts. The rate of change of the composition also revealed greater stability in the Pd−Pt[0.7]/C catalyst than in the Pd−Pt[0.5]/C catalyst, which was in good accordance with the EDX results. XPS element mapping was conducted to visualize the difference in the Pd:Pt composition of the Pd−Pt/C catalysts before and after the ADT (Figure 7 and Table 1). In the XPS element mapping, Pd is shown in red, and Pt is shown in blue. The images before the ADT are similar; however, after the ADT, blue is the more dominant color in the Pd−Pt[0.5] image compared to the initial Pd−Pt[0.7] image. In addition, the image of Pd−Pt[0.7] after the ADT is similar to the initial Pd−Pt[0.7] image. These results also indicate that Pd dissolution occurred in the Pd−Pt/C and that the Pd−Pt[0.7]/C catalyst was more stable than the Pd−Pt[0.5]/C catalyst. In situ electrochemical impedance spectroscopy (EIS) was performed to verify the changes in MEA resistance (Figure S8 in the Supporting Information).

4. CONCLUSIONS

In conclusion, we have demonstrated Pt-exoskeleton catalysts with high stability and remarkable activity and evaluated the degradation characteristics of these catalysts in MEAs using a

DOI: 10.1021/acsami.5b03255
ACS Appl. Mater. Interfaces 2015, 7, 14053−14063

load-cycling ADT. The Pt-exoskeleton catalysts yielded a noticeable improvement in the performance of the MEA, which is an actual fuel cell device. The Pt mass activity of Pd−Pt[0.5]/C and of Pd−Pt[0.7]/C were enhanced by factors of 2.04 and 1.56, respectively, over commercial Pt/C. In addition, these catalysts showed distinct degradation characteristics during an MEA load-cycling test, which was performed under more realistic fuel cell conditions than those created using a half-cell. The Pt/C MEA performance initially decreased rapidly over 0−10 h and then declined slowly and gradually, and this pattern occurred because Pt particle growth affected the ECSA loss. However, the MEA performance of Pt-exoskeleton catalysts was more stable than that of Pt/C MEA over 10 h because the Pd core stabilized the Pt exoskeleton. However, the Pd core began to dissolve because of imperfections in the Pt shell, and the dissolved Pd ions formed a Pd band within the electrolyte membrane. Consequently, a continuous decrease in the performance was observed later in the ADT. An intact shell is an important factor for enhancing the durability of core−shell structure catalysts. In future studies, we will investigate the optimum design of the Pt exoskeleton and dealloying of the base metal for practical fuel cell operating.

■ ASSOCIATED CONTENT

Supporting Information

ORR activity of commercial Pt/C and Pd−Pt/C catalyst in half-cell (Figure S1), other polarization curves (Figure S2), degradation ratio with various voltages at the specified time intervals during ADT (Figure S3), FE-SEM cross-section images of the MEAs (Figure S4), and other analysis (EDX, ERD, XPS, EIS) of the MEAs, XPS analysis, and evaluation of Pt-exoskeleton (shell) thickness. The Supporting Information is available free of charge on the ACS Publications website at DOI: 10.1021/acsami.5b03255.

■ AUTHOR INFORMATION

Corresponding Authors

*E-mail: yhun00@gmail.com. Tel: 82-33-570-6546. Fax: 82-33-570-6535.

*E-mail: ysung@snu.ac.kr. Co-Tel: 82-2-880-1889. Fax: 82-2-888-1604.

Author Contributions

The manuscript was written through contributions of all authors. All authors have given approval to the final version of the manuscript.

Notes

The authors declare no competing financial interest.

■ ACKNOWLEDGMENTS

This work was supported by Project Code IBS-R006-G1 in Korea. Y.-H. C. acknowledges financial support from the Basic Science Research Program (2013R1A1A2061636) through the National Research Foundation of Korea (NRF), which is funded by the Ministry of Education. This work was also supported by the NRF Grant funded by the Korean Government (MSIP) (2012R1A1A1041991).

■ REFERENCES

(1) Gasteiger, H. A.; Markovic, N. M. Just A Dream − or Future Reality? *Science* **2009**, *324*, 48−49.

(2) Su, D. S.; Sun, G. Nonprecious−Metal Catalysts for Low-Cost Fuel Cells. *Angew. Chem., Int. Ed.* **2011**, *50*, 11570−11572.

(3) Jaouen, F.; Jaouen, F.; Proietti, E.; Lefèvre, M.; Chenitz, R.; Dodelet, J.-P.; Wu, G.; Chung, H.; Taek; Johnston, C. M.; Zelenay, P. Recent Advances In Non-Precious Metal Catalysis For Oxygen-Reduction Reaction In Polymer Electrolyte Fuel Cells. *Energy Environ. Sci.* **2011**, *4*, 114−130.

(4) Wang, J. X.; Inada, H.; Wu, L.; Zhu, Y.; Choi, Y. M.; Liu, P.; Zhou, W.; Adzic, R. R. Oxygen Reduction On Well-Defined Core-Shell Nanocatalysts: Particle Size, Facet, And Pt Shell Thickness Effect. *J. Am. Chem. Soc.* **2009**, *131*, 17298−17302.

(5) Wang, D.; Xin, H. L.; Yu, Y.; Wang, H.; Rus, E.; Muller, D. A.; Abruna, H. D. Pt-Decorated PdCo@Pd/C Core-Shell Nanoparticles with Enhanced Stability and Electrocatalytic Activity for the Oxygen Reduction Reaction. *J. Am. Chem. Soc.* **2010**, *132*, 17664−17666.

(6) Antolini, E. Palladium in Fuel Cell Catalysis. *Energy Environ. Sci.* **2009**, *2*, 915−931.

(7) Zhang, H.; Jin, M.; Xia, Y. Enhancing The Catalytic and Electrocatalytic Properties of Pt-Based Catalysts by Forming Bimetallic Nanocrystals with Pd. *Chem. Soc. Rev.* **2012**, *41*, 8035−8049.

(8) Zhang, J.; Mo, Y.; Vukmirovic, M. B.; Klie, R.; Sasaki, K.; Adzic, R. R. Platinum Monolayer Electrocatalysts for O_2 Reduction: Pt Monolayer on Pd(111) and on Carbon-Supported Pd Nanoparticles. *J. Phys. Chem. B* **2004**, *108*, 10955−10964.

(9) Zhang, J.; Vukmirovic, M. B.; Xu, Y.; Mavrikakis, M.; Adzic, R. R. Controlling the Catalytic Activity of Platinum-Monolayer Electrocatalysts for Oxygen Reduction with Different Substrates. *Angew. Chem., Int. Ed.* **2005**, *44*, 2132−2135.

(10) Ruban, A.; Hammer, B.; Stoltze, P.; Skriver, H. L.; Nørskov, J. K. Surface Electronic Structure and Reactivity of Transition and Noble Metals. *J. Mol. Catal. A: Chem.* **1997**, *115*, 421−429.

(11) Hammer, B.; Nørskov, J. K. Theoretical Surface Science and Catalysis−Calculations and Concepts. *Adv. Catal.* **2000**, *45*, 71−129.

(12) Zhao, J.; Jarvis, K.; Ferreira, P.; Manthiram, A. Performance and Stability of Pd-Pt-Ni Nanoalloy Electrocatalysts in Proton Exchange Membrane Fuel Cells. *J. Power Sources* **2011**, *196*, 4515−4523.

(13) Borup, R.; Meyers, J.; Pivovar, B.; Kim, Y. S.; Mukundan, R.; Garland, N.; Myers, D.; Wilson, M.; Garzon, F.; Wood, D.; Zelenay, P.; More, K.; Stroh, K.; Zawodzinski, T.; Boncella, J.; McGrath, J. E.; Inaba, M.; Miyatake, K.; Hori, M.; Ota, K.; Ogumi, Z.; Miyata, S.; Nishikata, A.; Siroma, Z.; Uchimoto, Y.; Yasuda, K.; Kimijima, K. I.; Iwashita, N. Scientific Aspects of Polymer Electrolyte Fuel Cell Durability and Degradation. *Chem. Rev.* **2007**, *107*, 3904−3951.

(14) Darling, R. M.; Meyers, J. P. Kinetic Model of Platinum Dissolution in PEMFCS. *J. Electrochem. Soc.* **2003**, *150*, A1523−A1527.

(15) Yasuda, K.; Taniguchi, A.; Akita, T.; Ioroi, T.; Siroma, Z. Characteristics of a Platinum Black Catalyst Layer with Regard of Platinum Dissolution Phenomena in a Membrane Electrode Assembly. *J. Elctrochem. Soc.* **2006**, *153*, A1599−A1603.

(16) Colon-Mercado, H. R.; Popov, B. N. Stability of Platinum Based Alloy Cathode Catalysts in PEM Fuel Cells. *J. Power Sources* **2006**, *155*, 253−263.

(17) Gasteiger, H. A.; Kocha, S. S.; Sompalli, B.; Wagner, F. T. Activity Benchmarks and Requirements for Pt, Pt-Alloy, and Non-Pt Oxygen Reduction Catalysts for PEMFCS. *Appl. Catal. B: Environ.* **2005**, *56*, 9−35.

(18) Sasaki, K.; Naohara, H.; Cai, Y.; Choi, Y. M.; Liu, P.; Vukmirovic, M. B.; Wang, J. X.; Adzic, R. R. Core-Protected Platinum Monolayer Shell High Stability Electrocatalysts for Fuel Cell Cathodes. *Angew. Chem., Int. Ed.* **2010**, *49*, 8602−8607.

(19) Chen, Y.; Liang, Z.; Yang, F.; Liu, Y.; Chen, S. Ni-Pt Core-Shell Nanoparticles as Oxygen Reduction Electrocatalysts: Effect of Pt Shell Coverage. *J. Phys. Chem. C* **2011**, *115*, 24073−24079.

(20) Choi, R.; Choi, S.-I.; Choi, C. H.; Nam, K. M.; Woo, S. I.; Park, J. T.; Han, S. W. Designed Synthesis of Well-Defined Pd@Pt Core-Shell Nanoparticles with Controlled Shell Thickness As Efficient Oxygen Reduction Electrocatalysts. *Chem.—Eur. J.* **2013**, *19*, 8190−8198.

(21) Bae, S. J.; Kim, S. J.; Park, J. I.; Lee, J. H.; Cho, H.; Park, J. Y. Lifetime Prediction Through Accelerated Degradation Testing of

DOI: 10.1021/acsami.5b03255
ACS Appl. Mater. Interfaces 2015, 7, 14053−14063

Membrane Electrode Assemblies in Direct Methanol Fuel Cell. *Int. J. Hydrogen Energy* **2010**, *35*, 9166−9176.
(22) Lin, R.; Li, B.; Hou, Y. P.; Ma, J. M. Investigation of Dynamic Driving Cycle Effect on Performance Degradation and Micro-Structure Change of PEM Fuel Cell. *Int. J. Hydrogen Energy* **2009**, *34*, 2369−2376.
(23) Makaharia, R.; Kocha, S.; Yu, P.; Sweikart, A.; Gu, W.; Wagner, F.; Gasteiger, H. A. Durability and Reliability of Low-Temperature Fuel Cells Systems. *ECS Trans.* **2006**, *1*, 3−18.
(24) Jeon, T.-Y.; Pinna, N.; Yoo, S. J.; Ahn, D.; Choi, S. H.; Willinger, M.-G.; Cho, Y.-H.; Lee, K.-S.; Park, H.-Y.; Yu, S.-H.; Sung, Y.-E. Selective Deposition of Pt onto Supported Metal Clusters for Fuel Cell Electrocatalysts. *Nanoscaale* **2012**, *4*, 6461−6469.
(25) Kim, O.-H.; Cho, Y.-H.; Kang, S. H.; Park, H.-Y.; Kim, M.; Lim, J. W.; Chung, D. Y.; Lee, M. J.; Choe, H.; Sung, Y.-E. Ordered Macroporous Platinum Electrode And Enhanced Mass Transfer in Fuel Cells Using Inverse Opal Structure. *Nat. Commun.* **2011**, *4*, 2473.
(26) Bruijn, F. A.; Dam, V. A. T.; Janssen, G. J. M. Review: Durability and Degradation Issues of PEM Fuel Cell Components. *Fuel Cells* **2008**, *1*, 3−22.
(27) Zhang, S.; Yuan, X.; Hin, J. N. C.; Wang, H. A Review of Platinum-Based Catalyst Layer Degradation in Proton Exchange Membrane Fuel Cells. *J. Power Sources* **2009**, *194*, 588−600.
(28) Zhang, S.; Yuan, X.; Wang, H.; Merida, W.; Zhu, H.; Shen, J.; Wu, S.; Zhang, J. A Review Of Accelerate Stress Tests of MEA Durability in PEM Fuel Cells. *Int. J. Hydrogen Energy* **2009**, *34*, 388−404.
(29) Cho, Y.-H.; Jeon, T. Y.; Yoo, S. J.; Lee, K. S.; Ahn, M.; Kim, O.-H.; Cho, Y. H.; Lim, J. W.; Jung, N.; Yoon, W. S.; Choe, H.; Sung, Y.-E. Stability Characteristics of Pt_1Ni_1/C as Cathode Catalysts in Membrane Electrode Assembly of Polymer Electrolyte Fuel Cell. *Electrochim. Acta* **2012**, *59*, 264−269.
(30) Cho, Y.-H.; Lim, J. W.; Kang, Y. S.; Cho, Y. H.; Kim, O.-H.; Kwon, N. H.; Kwon, O. J.; Yoon, W. S.; Choe, H.; Sung, Y.-E. The Dependence of Performance Degradation of Membrane Electrode Assembly on Platinum Loading In Polymer Electrolyte Membrane Fuel Cell. *Int. J. Hydrogen Energy* **2012**, *37*, 2490−2497.
(31) Colon-Mercado, H. R.; Kim, H.; Popov, B. N. Durability Study of Pt_3Ni_1 Catalysts as Cathode in PEM Fuel Cells. *Electrochem. Commun.* **2004**, *6*, 795−799.
(32) Dubau, L.; Durst, J.; Marillard, F.; Guetaz, L.; Chtenet, M.; Andre, J.; Rossinot, E. Further Insights into the Durability of Pt_3Co/C Electrocatalysts: Formation of "Hollow" Pt Nanoparticles Induced By the Kirkendall Effect. *Electrochim. Acta* **2011**, *56*, 10658−10667.
(33) Wang, J. X.; Ma, C.; Choi, Y. M.; Su, D.; Zhu, Y.; Liu, P.; Si, R.; Vukmirovic, M. B.; Zhang, Y.; Adzic, R. R. Kirkendall Effect and Lattice Contraction in Nanocatalysts: A New Strategy to Enhance Sustainable Activity. *J. Am. Chem. Soc.* **2011**, *133*, 13551−13557.
(34) Zhao, D.; Xu, B.-Q. Enhancement of Pt Utilization in Electrocatalysts by Using Gold Nanoparticles. *Angew. Chem., Int. Ed.* **2012**, *51*, 68−89.

DOI: 10.1021/acsami.5b03255
ACS Appl. Mater. Interfaces 2015, 7, 14053−14063